XXII Congresso Brasileiro de Mecânica dos Solos e Engenharia Geotécnica
XI Simpósio Brasileiro de Engenheiros Geotécnicos Jovens
24 a 28 de agosto de 2026 – Brasília/DF
DOI: 10.47094/COBRAMSEG2026.5/68

Fragility Assessment of Pile Foundations under Liquefaction-Induced Lateral Spreading Using Random Fields in PLAXIS 3D

Bernardo Jiménez
Engenheiro geotecnista, Ulteig, Costa Rica, bernardo.jimenez@ulteig.com
Research fellow, Engenharia de Estruturas e Geotécnica (PEF), Universidade de São Paulo (USP), Brasil, bernardo.jimenez@alumni.usp.br.

Adrian Torrico Siacara
Professor, Engenharia de Estruturas e Geotécnica (PEF), Universidade de São Paulo (USP), São Paulo, Brasil, adrian.torrico@usp.br

ABSTRACT: Seismic performance assessment of pile foundations requires explicit consideration of the spatial variability of soil properties, as it strongly influences structural demand under liquefaction-induced lateral spreading. This study presents a probabilistic framework for the derivation of fragility curves for drilled shaft foundations subjected to lateral spreading, combining three-dimensional finite-element analyses in PLAXIS 3D with lognormal random field modeling. Spatial variability of key geotechnical parameters is represented through covariance-based random fields incorporated into a user-defined soil model. A series of quasi-static numerical simulations is performed by imposing free-field lateral ground displacements representative of liquefaction-induced spreading over a wide range of intensity measures. Engineering demand parameters, including pile-head displacement, axial load, bending moment, curvature, and damage extent along the pile length, are extracted from 100 random-field realizations per intensity level. Damage states are defined based on moment–curvature analysis, and exceedance probabilities are used to derive lognormal fragility functions through maximum likelihood estimation. The results demonstrate that lateral spreading can induce significant axial–flexural interaction and distributed damage along the piles, even when the liquefiable layer and overlying crust are relatively thin compared to the total pile length. Fragility analysis is shown to be an effective approach for synthesizing large sets of numerical simulations into probabilistic performance metrics, supporting risk-consistent and performance-based seismic design of pile foundations in liquefaction-prone environments.

KEYWORDS: Liquefaction, lateral spread, random fields, fragility analysis, drilled shafts

1 INTRODUCTION

Liquefaction-induced lateral spreading represents one of the most critical seismic hazards for pile-supported structures, as it can impose large kinematic demands that are not adequately captured by inertial-based design approaches. Field observations from past earthquakes have shown that piles may experience significant axial–flexural interaction, stiffness degradation, and distributed damage even when liquefiable layers are relatively shallow (Tokimatsu & Asaka, 1998, Abdoun & Dobry, 2002). Consequently, reliable assessment of pile performance under lateral spreading requires numerical frameworks capable of representing soil–structure interaction and inherent geotechnical uncertainty.

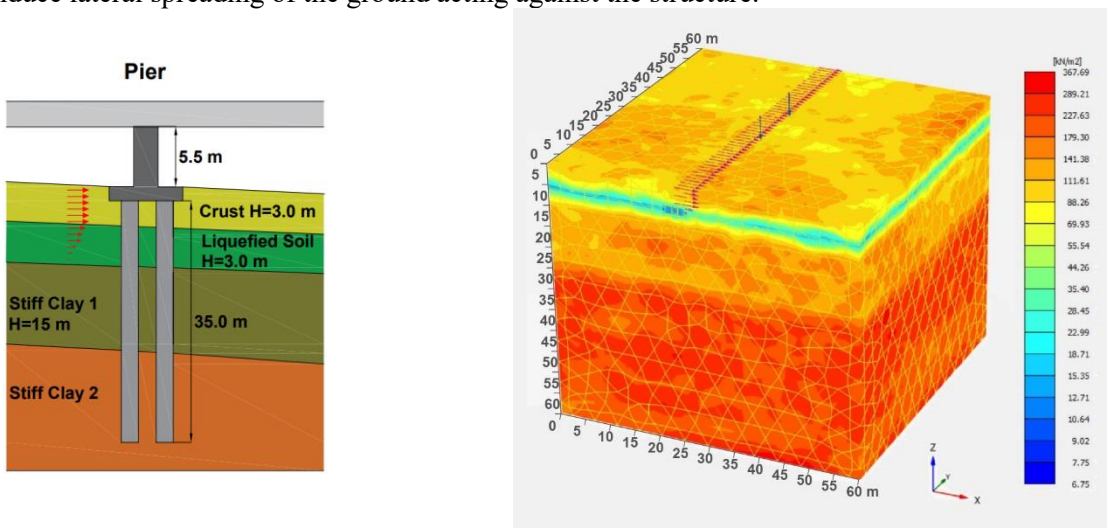
Conventional deterministic analyses commonly rely on single-valued soil profiles and prescribed ground deformation patterns, which may lead to biased or non-conservative estimates of structural demand. A first type of probabilistic extension consists of modeling soil properties as random variables (RV), which allows the inherent variability of geotechnical materials to be considered, although without accounting for spatial variability (Wyjadłowski, 2026). In contrast, probabilistic approaches that incorporate random fields, incorporates spatial variability of soil properties, which allow a more realistic description of ground response and its impact on deep foundations. Random field (RF) modeling has emerged as an effective tool to represent spatial uncertainty in geotechnical parameters, while fragility analysis provides a consistent means to translate large sets of numerical simulations into probabilistic measures of structural damage and performance. Recent studies have demonstrated the effectiveness of probabilistic frameworks for evaluating geotechnical system

performance under complex loading conditions, particularly when uncertainty and nonlinear soil behavior govern the response (Siacara et al., 2024a, Siacara et al., 2024b). These approaches provide a rational basis for quantifying damage and performance beyond deterministic assessments.

In this context, the present study proposes a fragility-based assessment framework for pile foundations subjected to liquefaction-induced lateral spreading, combining covariance-based RFs with three-dimensional finite-element modeling using the commercial software PLAXIS 3D (Bentley Systems, 2024). The methodology is applied to a highway overpass pier supported by drilled shafts in Costa Rica, enabling the evaluation of axial load redistribution, bending demand, damage state development, and damage extent along the pile length. The results illustrate the suitability of fragility analysis as a practical and robust approach for interpreting complex soil–structure interaction simulations and for supporting performance-based seismic design of pile foundations in liquefaction-prone environments.

2 BACKGROUND

The case study corresponds to the Taras overpass intersection, located in Cartago, Costa Rica. The structure consists of a pier system supported by six drilled shafts with a diameter of 1.2 m and a total embedment depth of 35.0 m. Construction of the project began in 2021, and the structure was placed into operation in 2024. Regarding subsurface conditions, as presented in Figure 1 a), a layer of sandy silt was identified at an approximate depth of 3.0 m. Under seismic loading, this layer presents liquefaction potential, which may induce lateral spreading of the ground acting against the structure.



a) b)

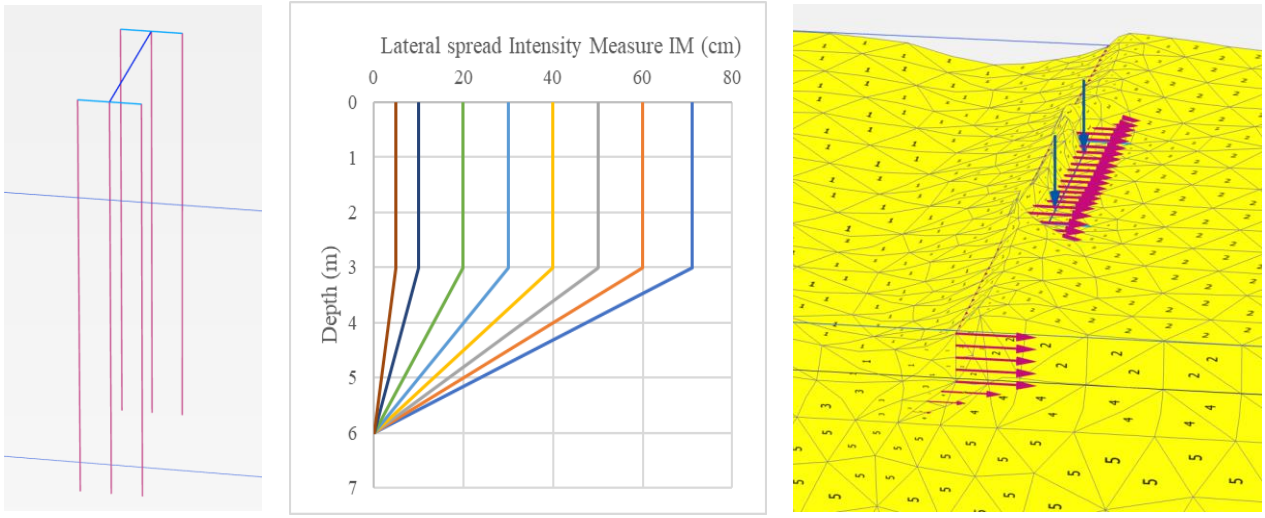
Figure 1. a) *Idealized soil profile and drilled shaft foundation subjected to lateral spreading b) Random fields model showing the liquefied layer with correlations lengths Lx=Ly=12 & Lz=2.*

3 APPLIED METHODOLOGY

In this study, RF was employed to simulate the lateral spreading of the ground acting against the structure. PLAXIS 3D was used to evaluate forces and deformations in the soil–structure system. The spatial variability of soil properties was incorporated by coupling the RF model with a user-defined soil model (UDSM) implemented in PLAXIS 3D. The random fields were generated in Python following a covariance-based approach. Figure 1(b) shows an example of a generated random field.

For each intensity measure (IM), 100 numerical simulations were performed with a different RF. Finally, the fragility analysis was performed from the database was post-processed and analyzed using RStudio, which specializes in data analysis. Figure 2 illustrates several key aspects of the numerical modeling. Figure 2 (a) presents the configuration of six drilled shafts (1.2 m diameter) supporting the pier, consisting of two front shafts, two middle shafts, and two rear shafts. Figure 2 (b) shows the IM values adopted in the analyses, with a maximum value of 71 cm under free-field conditions determined by Jimenez (2023), following the methodology of lateral spread analysis proposed by CALTRANS (2012), assuming constant deformation

within the crust layer and a gradual deformation profile within the liquefiable layer. Finally, Figure 2 c) illustrates the proper modeling of lateral spreading, where the soil mass is observed to impact the pier, inducing upward sliding of the crust layer.



a) b) c)

Figure 2. a) *Pile-pier systems b) Intensity Measures used c) Lateral spreading soil deformation acting on the pile.*

Table 1. Assumed properties in random field.

Stage	Service						Liquefaction			
Soil	**Cohesion (kPa)**	**σ (kPa)**	**Friction angle (°)**	**σ (°)**	**E (kPa)**	**σ (kPa)**	**Undrained shear strength Su (kPa)**	**σ (kPa)**	**E (kPa)**	**σ (kPa)**
Crust	10	2	28	2	20000	2000	100	20	30000	1500
Liquefied soil	5	1	25	2	15000	1500	12	3	2400	200
Stiff clay 1	20	3	35	3	40000	2500	120	20	36000	2500
Stiff clay 2	40	4	38	3	60000	3000	230	30	69000	2500

4 RANDOM FIELD GENERATION

The spatial variability of soil properties was represented using a random-field approach based on a covariance formulation. As presented by Zhang et al. (2023), a target covariance function was defined to describe the spatial correlation of the selected soil parameters, allowing the generation of statistically consistent realizations of the ground deformation associated with lateral spreading. The covariance between two points separated by a distance r was expressed as

$$C(r) = \sigma^2 \exp\left(-\frac{r}{\theta}\right) (1)$$

where $\sigma^2$is the variance of the parameter and θ is the correlation length governing spatial continuity. The random fields were generated through Cholesky decomposition of the covariance matrix to ensure the prescribed spatial correlation structure. The parameters adopted for the random-field generation are summarized in Table 1, obtained from calibrated triaxial test and CPT tests, where a clear discretization is introduced between the loading phase, modeled under effective stress conditions, and the liquefaction phase, modeled under total stress conditions.

5 MOMENT–CURVATURE ANALYSIS AND DEFINITION OF DAMAGE STATES

The sectional flexural response of the pile was characterized through moment–curvature (M–κ) relationships computed for multiple axial force levels. Curvature, κ, was defined as the second derivative of the lateral displacement $w(z)$, and under the assumption of plane sections remaining plane, it may be expressed as the strain difference between extreme fibers divided by their separation. In the elastic range, the flexural response follows the linear relation $M = EI\kappa$, while nonlinear behavior develops once cracking or yielding occurs.

Moment–curvature analyses were performed for a wide range of axial forces, including both compression and tension, explicitly accounting for axial–flexural interaction effects. Axial load was found to significantly influence both flexural strength and ductility: moderate compressive axial force may increase moment capacity but reduces curvature ductility, whereas tensile axial force leads to a pronounced reduction in flexural capacity and deformation reserve.

Based on the computed M–κ relationships, two damage states were defined. Damage State 1 (DS1) corresponds to the knee point of the response curve, (M_k, κ_k), identified by the end of the linear elastic behavior, a marked reduction in flexural stiffness and association with the initiation of cracking in the section. Damage State 2 (DS2) corresponds to the maximum bending moment capacity, $M_{\max}$, representing the upper limit of flexural resistance for a given axial force. The ultimate curvature, κ_u, characterizes the deformation capacity of the section prior to instability or failure (Calvi et al., 2007).

As seen in Figure 3 presents representative M–κ curves obtained using the commercial software LPile (Ensoft, Inc., 2015), illustrating the influence of axial force on both moment capacity and post-elastic behavior for a 1.2 m diameter drilled shaft. These moment–curvature relationships provide the mechanical basis for the definition of damage thresholds adopted in the subsequent fragility analysis.

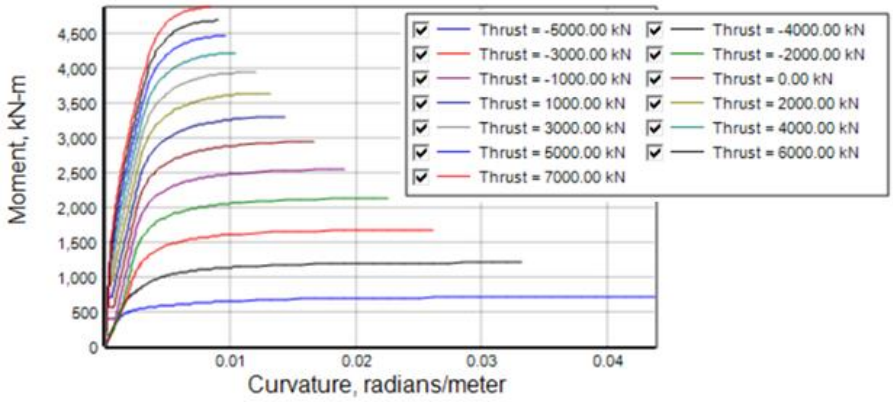


Figure 3. Moment–curvature response of the pile section considering axial–flexural interaction effects.

6 FRAGILITY ANALYSIS

Fragility functions were developed to quantify the probability of exceeding a given damage state DS_i conditioned on the lateral spreading intensity measure (IM). This method has proven to be an efficient method for evaluating damage in pile foundations (Basu, 2012, Basu et al. (2020). The fragility curves were assumed to follow a lognormal distribution, such that the conditional probability of exceedance is expressed as

$$P[DS \geq DS_i \mid IM] = \Phi\left(\frac{\ln(IM) - \ln(\mu_i)}{\beta_i}\right) \quad (2)$$

where $\Phi(\cdot)$ is the standard normal cumulative distribution function, μ_i is the median value of IM associated with damage state DS_i, and β_i is the logarithmic standard deviation. The parameters μ_i and β_i were estimated using a maximum likelihood approach, based on binary outcomes of damage exceedance obtained from the numerical simulations. For each simulation j, the likelihood function was defined as

$$\mathcal{L}(\mu_i, \beta_i) = \prod_{j=1}^{N} \left[{P_j}^{\delta_j} (1 - P_j)^{1-\delta_j} \right] \quad (3)$$

where $P_j = P\left[DS \geq DS_i \mid IM_j\right]$ and δ_j is an indicator variable equal to 1 if the damage state was exceeded and 0 otherwise. Separate fragility functions were derived for each damage state (DS1 and DS2), providing a probabilistic description of pile performance under liquefaction-induced lateral spreading.

7 OBTAINED RESULTS

The following results correspond to 100 RF simulations performed for each IM considered. Being this a symmetric pile geometry problem, representative conditions for a front, middle, and rear pile were analyzed. Figure 4 presents the relationship between ground displacement, definied by the IM and pile-head displacement, with results summarized using boxplots. Similar orders of magnitude in pile-head displacement are observed for all piles, which is attributed to the pile cap rigidly connecting the pile heads. The middle piles exhibit narrower interquartile ranges compared to the front and rear piles, although the presence of outliers was also observed, likely associated with variability in axial load response, as discussed later. For lower IM levels (1.0–5.0 cm), the dispersion of results is limited, reflecting ground displacements that do not induce flexural stiffness degradation and therefore lead to similar responses across simulations. As ground deformation increases, pile-head displacement tends to stabilize, reaching an asymptotic value of approximately 14.8 cm for an IM of 71 cm.

The variation of axial load in the piles for the different IMs is illustrated in Figure 5, where compressive forces are reported as negative values and tensile forces as positive values. For the front pile, only the IM of 5 cm results in compressive axial load; for all other IMs, the pile is subjected to axial tension, indicating that uplift induced by lateral spreading exceeds the gravitational load of the superstructure. For larger IMs, axial tensile forces tend to stabilize at values of approximately 3600 kN. The middle pile exhibits relatively stable compressive axial loads with limited dispersion for IMs up to 40 cm, as reflected by narrow boxplots; beyond this threshold, a more erratic response is observed, with mean values shifting toward axial tension. In contrast, the rear pile experiences the largest compressive axial loads, acting to counterbalance the uplift of the pile cap induced by lateral spreading in the other piles, with compression forces reaching up to approximately an average of 6600 kN for the highest IM levels.

The relationship between axial load and peak bending moment in the piles is shown in Figure 6. Approximately linear trends are observed between axial force and bending moment for all pile locations. The front pile, which is predominantly subjected to axial tension, reaches peak bending moments exceeding 8000 kNm for the largest IM levels. For the middle pile, the axial force–moment relationship exhibits a steeper slope under tensile axial forces than under compressive forces, indicating a stronger sensitivity of flexural demand to tension. In contrast, the rear pile, which is primarily under axial compression, develops the highest bending moments, with peak values exceeding 12,000 kNm, reflecting the larger magnitude of compressive axial forces compared to the tensile forces experienced by the front pile. Additionally, the relationship between IM and bending moment is clearly nonlinear: bending moments associated with an IM of 40 cm are not twice those obtained for an IM of 20 cm, and increasing IM levels tend to produce progressively similar bending moments, indicating a saturation of flexural demand at large ground deformations.

The results of the fragility analysis are illustrated in Figure 7. For Damage State 1 (DS1), associated with the cracking moment, all simulations indicate a non linear behavior for ground displacements as low as 5 cm, as the cracking moment was achieved, reflecting the onset of flexural stiffness degradation. For Damage State 2 (DS2), the most critical response corresponds to the rear pile, which sustains the largest bending moment demands; in this case, the intensity range at which all simulations reach plastic hinge formation lies between 5 and 10 cm. For the front and middle piles, this transition occurs at higher intensity levels, between 10 and 20 cm. These results highlight the severity of liquefaction-induced lateral spreading, where the impact of a moving soil mass against the foundation system can generate significant structural demand. To further assess the consequences of plastic hinge formation, Figure 8 presents the relationship between peak bending moment and maximum curvature. The maximum curvature attained in all cases ranges approximately between 0.004 and 0.005, which remains below the ultimate curvature limit κ_u of the least ductile pile section shown in Figure 3 ($\kappa_u \approx 0.008$). This indicates that, although significant deformation develops during lateral spreading and the pile section would develop plastic strains across its cross-section, no structural failure of the element would occur.

Finally, the spatial extent of damage along the pile length was investigated through a fragility-based analysis presented in Figure 9. For Damage State 1 (DS1), it is observed that for an IM of 5 cm, cracking-related damage extends over approximately 2.0 m along the pile; for an IM of 20 cm, the damaged length exceeds 7.5 m; and for larger IMs, damage is observed over more than 10 m of the pile. These regions correspond to sections reaching the cracking moment, where flexural stiffness degradation is expected. For

Damage State 2 (DS2), associated with plastic hinge formation, the extent of damage is initially limited: for an IM of 5 cm, the affected length is approximately 0.06 m. However, an IM of 20 cm leads to plastic hinge formation over an extension of approximately 2.5 m with a probability of 75 %. For the largest IM considered (71 cm), there is an almost 100% probability of plastic hinge formation over at least 2.5 m of the pile, a 50 % probability of extending over at least 3.0 m, and a 25 % probability of affecting up to 6.0 m of the pile length. These results further highlight the severity of liquefaction-induced lateral spreading, particularly considering that in this case the liquefiable layer thickness and the overlying crust impacting the structure are both approximately 3.0 m, which are relatively small compared to the total pile length of 35 m.

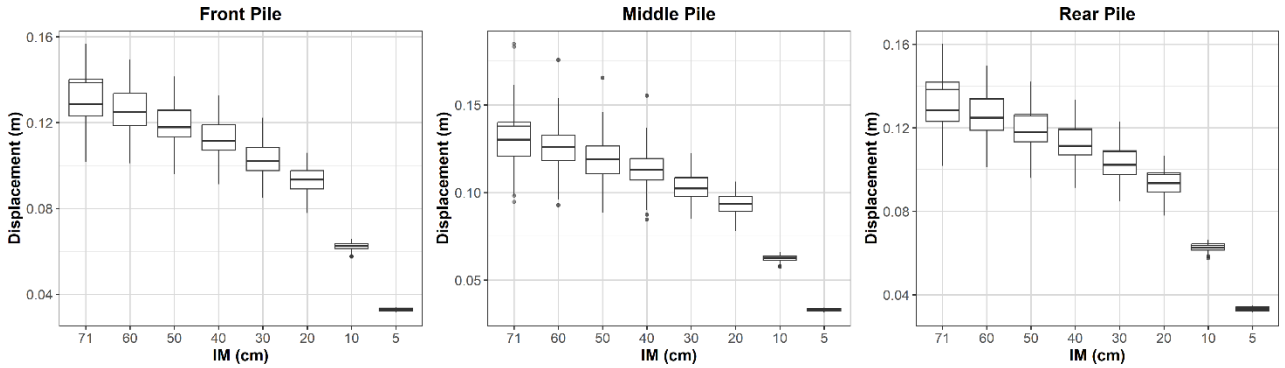


Figure 4. Pile head displacement vs ground deformation.

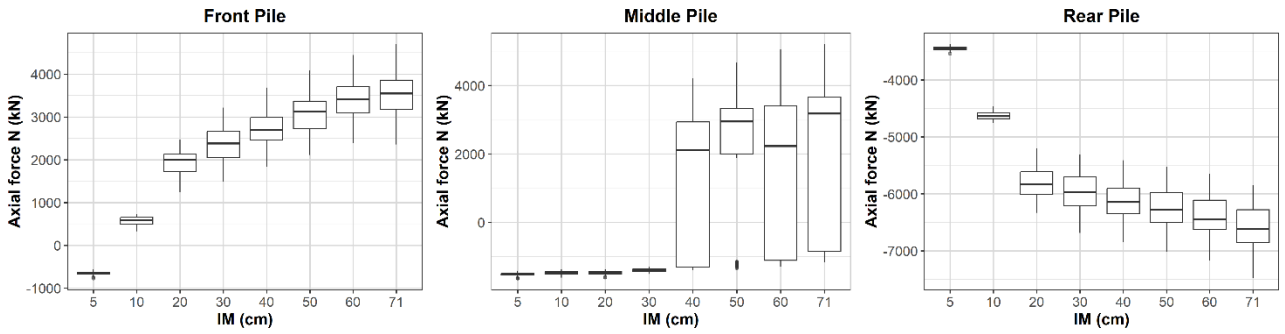


Figure 5. Axial loads bloxplots at pile head. Tension loads positives, compression loads negative.

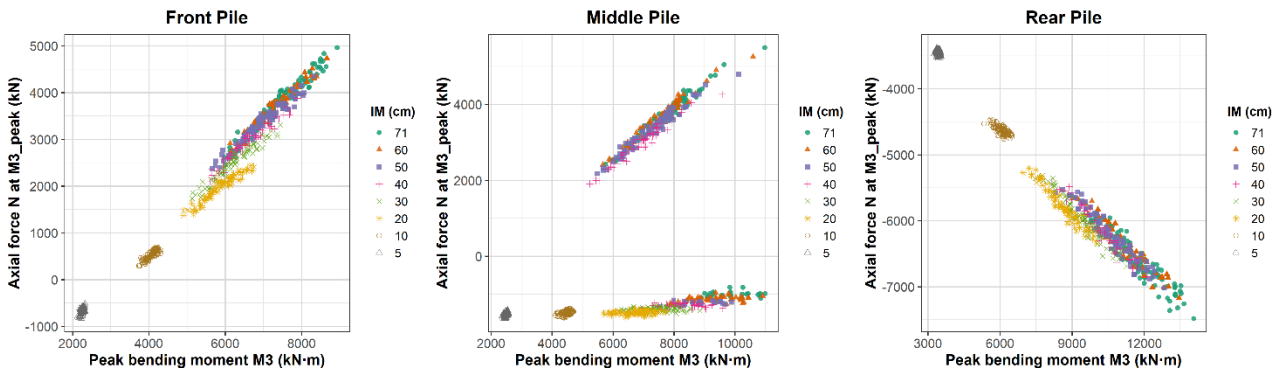


Figure 6. Peak bending moment vs corresponding axial load.

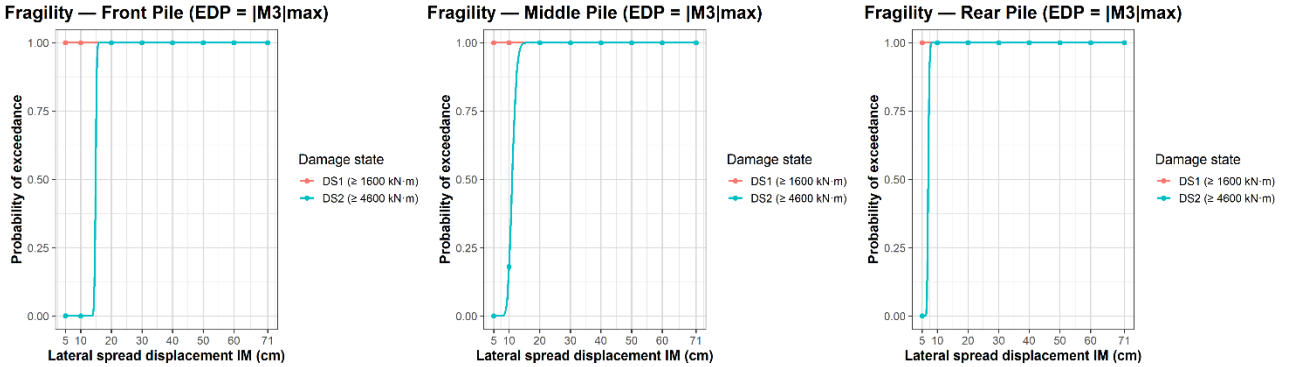


Figure 7. Fragility curves for DS1 & DS2.

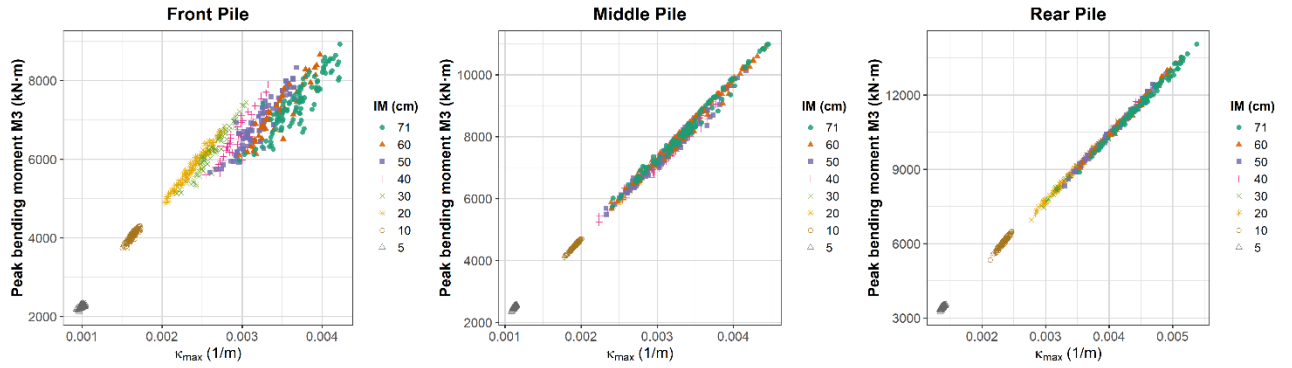


Figure 8. Peak moment vs max curvature κ.

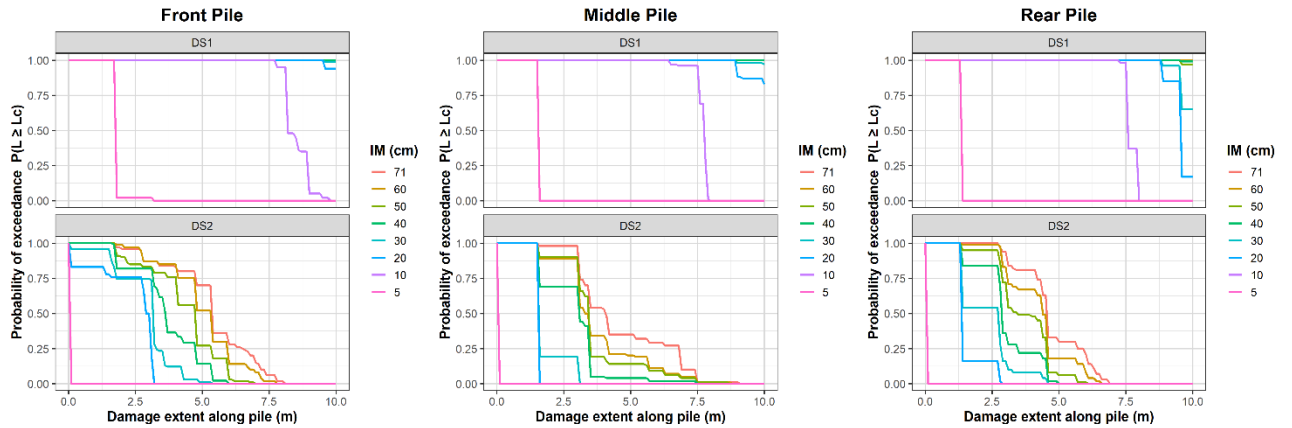


Figure 9. Damage extent fragility by IM | Facets: DS1 (cracking moment) DS2 (maximum bending moment).

8 CONCLUSIONES

This study presented a probabilistic framework for evaluating the seismic performance of pile foundations subjected to liquefaction-induced lateral spreading, explicitly accounting for the spatial variability of soil properties through random fields (RF). The adopted approach demonstrates that fragility analysis provides an effective and robust tool for synthesizing large sets of numerical simulations into meaningful performance metrics, allowing structural damage to be quantified in probabilistic terms rather than through isolated deterministic responses.

The results show that lateral spreading can induce significant axial–flexural interaction effects in pile foundations, even when the liquefiable layer and overlying crust are relatively thin compared to the total pile length. Although the rigid pile cap leads to similar pile-head displacements among all piles, marked differences in axial load and bending moment demands were observed, with rear piles experiencing the most critical compressive and flexural demands.

Moment–curvature analyses confirmed that axial force strongly governs both flexural strength and ductility. Damage State 1 (DS1), associated with cracking and stiffness degradation, was reached at relatively low intensity measures (IM ≈ 5 cm), while Damage State 2 (DS2), associated with plastic hinge formation, occurred at lower IM levels for rear piles than for front and middle piles. Fragility curves further demonstrated that damage is not only more likely at higher IMs but also progressively distributed along the pile length, revealing the potential for extended plastic regions rather than localized failure.

Despite the development of significant plastic strains during lateral spreading, maximum curvature demands remained below the ultimate curvature capacity of the pile sections, indicating that global structural failure is unlikely for the conditions analyzed. Overall, the study confirms that fragility-based assessment, coupled with random field modeling, constitutes a suitable and efficient framework for interpreting complex soil–structure interaction simulations, supporting performance-based design and risk-informed decision-making for pile-supported structures in liquefaction-prone environments.

9 REFERENCES

Abdoun, T., & Dobry, R. (2002). Evaluation of pile foundation response to lateral spreading. *Soil Dynamics and Earthquake Engineering*, *22*(9-12), 1051-1058.

Basu, P (2012). Fragility Analysis of Nondisplacement Piles in Sand. In *GeoCongress 2012: State of the Art and Practice in Geotechnical Engineering* (pp. 4290-4298).

Basu, P., Basu, S. B., & Ghasemi-Fare, O. (2020). Fragility analysis of drilled shafts in sand–an analytical correspondence between reliability index and factor of safety. *Soils and Foundations*, *60*(5), 1112-1130.

Bentley Systems. (2024). *PLAXIS 3D* (Version 2024.3) [Computer software]. Bentley Systems. https://www.plaxis.com

California Department of Transportation (Caltrans). (2012). *Guidelines on foundation loading and deformation due to liquefaction-induced lateral spreading.*.

Calvi, G. M., Priestley, M. J. N., & Kowalsky, M. J. (2007, December). Displacement-based seismic design of structures. In *New Zealand conference on earthquake engineering* (Vol. 2007). IUSS press.

Ensoft, Inc. (2015). *LPILE* (Version 2015) [Computer software]. Ensoft, Inc. https://www.ensoftinc.com

Jimenez, B.J. (2023). *Lateral spreading evaluation and mitigation for highway overpass structure Taras, Cartago, Costa Rica*. DFI 48th Annual Conference on Deep Foundations, Deep Foundations Institute, New York, NY; pp. 371-382.

Siacara, A. T., Beck, A. T., & Ji, J. (2024). Impact of random field simulations on FEM-based earth slope reliability. *Geotechnical and geological engineering*, *42*(8), 7873-7891.

Siacara, A. T., Guo, X., & Beck, A. T. (2024). Probabilistic analysis of shallow foundation on earth slope using an active learning surrogate-centered procedure. *Computers and Geotechnics*, *175*, 106659.

Tokimatsu, K., & Asaka, Y. (1998). Effects of liquefaction-induced ground displacements on pile performance in the 1995 Hyogoken-Nambu earthquake. Soils and Foundations, 38, 163-177.

Wyjadłowski, M. (2025). Lateral Loaded Pile Reliability Analysis Using the Random Set Method. *Buildings*, *15*(6), 882.

Zhang, J., Xiao, T., Ji, J., Zeng, P., & Cao, Z. (2023). *Geotechnical reliability analysis*. Singapore: Springer.